

Transmon-based simulator of nonlocal electron-phonon coupling: a platform for observing sharp small-polaron transitions

Vladimir M. Stojanović^{†,1} Mihajlo Vanević,² Eugene Demler,¹ and Lin Tian^{‡3}

¹*Department of Physics, Harvard University, Cambridge, MA 02138, USA*

²*Department of Physics, University of Belgrade, Studentski Trg 12, 11158 Belgrade, Serbia*

³*School of Natural Sciences, University of California, Merced, California 95343, USA*

(Dated: August 14, 2018)

We propose an analog superconducting quantum simulator for a one-dimensional model featuring momentum-dependent (nonlocal) electron-phonon couplings of Su-Schrieffer-Heeger and “breathing-mode” types. Because its corresponding coupling vertex function depends on both the electron- and phonon quasimomenta, this model does not belong to the realm of validity of the Gerlach-Löwen theorem that rules out any nonanalyticities in single-particle properties. The superconducting circuit behind the proposed simulator entails an array of transmon qubits and microwave resonators. By applying microwave driving fields to the qubits, a small-polaron Bloch state with an arbitrary quasimomentum can be prepared in this system within times several orders of magnitude shorter than the typical qubit decoherence times. We demonstrate that – by varying the externally-tunable parameters – one can readily reach the critical coupling strength required for observing the sharp transition from a nondegenerate (single-particle) ground state corresponding to zero quasimomentum ($K_{\text{gs}} = 0$) to a twofold-degenerate small-polaron ground state at nonzero quasimomenta K_{gs} and $-K_{\text{gs}}$. Through exact numerical diagonalization of our effective Hamiltonian, we show how this nonanalyticity is reflected in the relevant single-particle properties (ground-state energy, quasi-particle residue, average number of phonons). We also show that the proposed setup provides an ideal testbed for studying the nonequilibrium dynamics of small-polaron formation in the presence of strongly momentum-dependent electron-phonon interactions.

PACS numbers: 85.25.Cp, 03.67.Ac, 71.38.Ht

I. INTRODUCTION

Based on the pioneering ideas of Feynman and Lloyd^{1,2}, and bolstered by developments in technology and methods for manipulation and control, the field of quantum simulation is at the current frontier of physics research³. Its overarching goal is to help us understand the behavior of complex quantum many-body systems by studying their simpler, highly-controllable counterparts. The field has already matured enough to allow realizations of various quantum spin models, models with bosonic degrees of freedom, and even of those that go beyond the conventional low-energy physics paradigm⁴. In particular, polaronic systems have quite recently attracted attention among researchers in the field, as evidenced by the proposals for simulating such systems with trapped ions^{5,6}, cold polar molecules^{7,8}, Rydberg atoms or ions⁹, and superconducting (SC) circuits¹⁰.

Conceived by Landau and Pekar as a by-product of their investigation of charge carriers in polar semiconductors¹¹, the polaron concept has played a pivotal role in studies of electron-phonon (e-ph) interaction ever since¹². It envisions an excess carrier (electron, hole) in a narrow-band semiconductor (or an insulator) strongly interacting with the host-crystal lattice vibrations. The effective

mass of the carrier is increased – compared to the bare-band value – due to a self-induced lattice deformation that causes an effective “dressing” of the carrier by virtual phonons (self-trapping). Polaronic carriers have been found in materials ranging from amorphous semiconductors^{13,14} to colossal-magnetoresistive oxides¹⁵ to undoped cuprates¹⁶. More recently, polaronic behavior has been identified in cold-atomic systems¹⁷. Besides, the generalized polaron concept includes almost any instance of a quantum particle strongly coupled to a bosonic environment, giving rise to a field-theoretic model of a fermion interacting with a scalar boson field.

In systems with short-range e-ph coupling, a typical size of the phonon cloud around a carrier does not exceed a unit cell of the host crystal (small polarons). Such carriers are usually studied within the framework of the Holstein molecular-crystal model, a paradigm for the polaron-crossover problem¹⁸. It describes purely local – hence momentum-independent – interaction of tightly-bound electrons with dispersionless (Einstein) phonons. Owing to a large body of work over the past five decades¹², both static and dynamical properties of this model are well understood by now. Recent small-polaron studies have, however, focussed on strongly momentum-dependent e-ph interactions¹⁹. An important example is furnished by Su-Schrieffer-Heeger (SSH) coupling (also known as Peierls-type or off-diagonal coupling), which accounts for the dependence of electronic hopping integrals upon phonon states and has a significant bearing on transport properties of π -electron sys-

[†]Electronic mail: stojanovic@physics.harvard.edu

[‡]Electronic mail: ltian@ucmerced.edu

tems, such as organic semiconductors²⁰, carbon nanotubes²¹, and graphene-based nanostructures²². Such strongly momentum-dependent couplings, with vertex functions that depend both on the electron and phonon quasimomenta, are also relevant for fundamental reasons. Namely, they do not belong to the realm of validity of the Gerlach-Löwen theorem²³, which asserts that (single-particle) e-ph models generically show smooth dependence of the ground-state energy on the coupling strength. While this theorem was long believed to be of quite general validity, it applies only to momentum-independent (Holstein-like) couplings and those that do depend on the phonon- but not on the electron quasimomentum. The latter are exemplified by the “breathing-mode” (BM) coupling²⁴, relevant in the cuprates.

The field of SC qubits²⁵ was revolutionized by the development of circuit quantum electrodynamics (circuit QED)^{26–28}, which allowed both fast quantum-gate realizations^{29,30} and demonstrations of many quantum-optics effects. Quite recently, circuit QED has come to the fore as a versatile platform for on-chip analog quantum simulation^{31,32}. Spurred by some recent advances in the realm of SC quantum devices, especially the striking increase in achievable coherence times of transmon qubits (from 1 μ s to nearly 100 μ s)^{33,34}, theoretical proposals have already been set forth for simulating Bose-Hubbard-type models^{35–37}, coupled-spin^{38–40} and spin-boson models^{41,42}, topological states of matter⁴³, and gauge fields⁴⁴. Along similar lines, in this paper we propose an SC-circuit emulation of a one-dimensional model featuring momentum-dependent e-ph couplings of SSH and BM types. This analog simulator entails SC transmon qubits and microwave resonators, the standard building blocks of circuit-QED systems⁴⁵. The role of qubits in our system is to emulate spinless-fermion excitations, where the pseudospin-1/2 operators representing the qubits are mapped to fermionic ones through the Jordan-Wigner transformation. At the same time, the resonator modes (microwave photons) play the role of dispersionless (Einstein) phonons.

We show that the suggested setup allows realization of strong e-ph coupling regime, characterized by a small-polaron formation. Furthermore, it enables the observation of a sharp transition from a nondegenerate single-particle ground state at zero quasimomentum to a twofold-degenerate one corresponding to a pair of equal and opposite (nonzero) quasimomenta. To demonstrate the feasibility of our simulation scheme, we show that – by applying appropriate pump pulses on the qubits – the relevant small-polaron states can be prepared within time scales several orders of magnitude shorter than the relevant qubit decoherence times.

The proposed simulator is particularly suitable for a detailed characterization of small-polaron ground states (or even excited states), by extracting their phonon content through direct counting of photons on the resonators. This unique tool, which is not at our disposal in traditional solid-state systems, also opens up the possibil-

ity to address experimentally the nonequilibrium aspects of polaron physics, i.e., the complex problem of polaron-formation dynamics^{46,47}. The question as to how rapidly upon creation (injection) of a single electron (hole), i.e., e-ph interaction quench, the cloud of correlated virtual phonons around it forms and results in a “dressed” polaronic quasiparticle is poorly understood at present. This dynamical process, which is expected to be particularly complex in systems with strongly momentum-dependent e-ph interactions, has quite recently attracted considerable attention^{48,49}.

The remainder of this paper is organized as follows. The layout of the simulator circuit is presented in Sec. II, together with the derivation of the effective Hamiltonian and discussion of the relevant parameter regime. In Sec. III, we first discuss the character of the momentum dependence of the simulated e-ph coupling, then some technical aspects related to exact numerical diagonalization, and finally, the results obtained for the small-polaron ground state. Special emphasis is placed on the occurrence of a sharp transition and the ensuing nonanalyticities in relevant single-particle properties (ground-state energy, quasiparticle residue, average number of phonons). Section IV starts with a brief description of our envisioned state-preparation protocol, followed by a discussion of the experimental-detection and robustness aspects of the simulator. In Sec. V we lay out the scheme for extracting the relevant retarded Green’s functions and the spectral function using the many-body Ramsey interference protocol. In addition, we explain in detail how our setup can be used for studying the dynamics of polaron formation. We summarize and conclude in Sec. VI.

II. ANALOG SIMULATOR AND ITS EFFECTIVE HAMILTONIAN

A. Circuit layout and underlying Hamiltonian

A schematic of the SC circuit behind the simulator is shown in Fig. 1. Each building block of the simulator consists of a transmon qubit (denoted as Q_n) and a SC resonator (R_n). The qubit emulates fermionic excitations, through mapping of its pseudospin-1/2 degree of freedom to spinless fermions via the Jordan-Wigner transformation. At the same time, the microwave photon modes of the SC resonator play the role of Einstein phonons. In this system, adjacent qubits couple to each other via a connecting circuit denoted as B_n . Contrary to the more familiar circuit-QED setup, the resonators here do not couple directly to the qubits. Instead, the magnetic flux of the resonator modes couples inductively to the connecting circuit B_n , which enables a nearest-neighbor XY-type qubit-qubit coupling whose strength depends on the quantum dynamics of the resonator modes.

The noninteracting Hamiltonian of the n -th repeating unit of the simulator, containing qubit Q_n and resonator

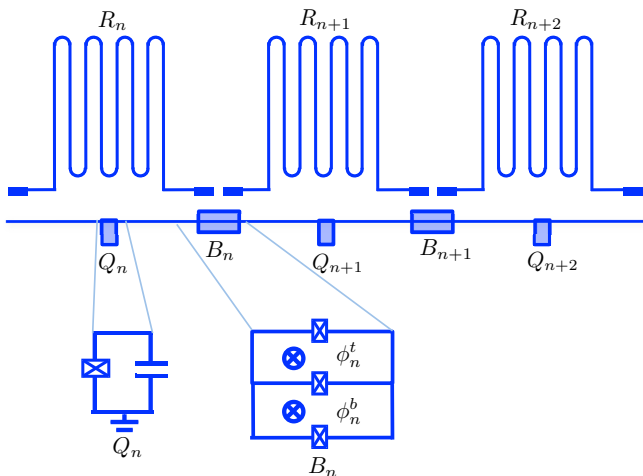


Figure 1: (Color online) Schematic of the simulator circuit containing transmon qubits Q_n , SC resonators R_n , and connecting circuits B_n with three Josephson junctions. External magnetic fluxes ϕ_n^b and ϕ_n^t are threading the bottom- and top loops of each connecting circuit, respectively. Note that the circuit elements are not drawn to scale.

R_n , can be written as

$$H_n^s = \hbar\omega_c a_n^\dagger a_n + \frac{E_z}{2} \sigma_n^z, \quad (1)$$

where E_z is the energy splitting of the qubit, and ω_c the frequency of the resonator mode; a_n (a_n^\dagger) is the annihilation (creation) operator for the modes of the resonator R_n , while the Pauli matrix σ_n^z represents the qubit Q_n .

The connecting circuit B_n consists of three Josephson junctions and can be viewed as a generalized SQUID loop. Let φ_n be the gauge-invariant phase variable of the SC island of the n -th qubit, and φ_n^i ($i = 1, 2, 3$) the respective phase drops on the three junctions in the circuit B_n . Based on flux-quantization rules⁵⁰, we then have

$$\begin{aligned} \varphi_n^1 &= \varphi_n - \varphi_{n+1} + \frac{\phi_n^t}{2}, \\ \varphi_n^2 &= \varphi_n - \varphi_{n+1} - \frac{\phi_n^t}{2}, \\ \varphi_n^3 &= \varphi_n - \varphi_{n+1} - \frac{\phi_n^t}{2} - \phi_n^b, \end{aligned} \quad (2)$$

where ϕ_n^t and ϕ_n^b are the respective magnetic fluxes in the top- and bottom loops of B_n ; both are expressed in units of $\Phi_0/2\pi$, where $\Phi_0 \equiv hc/(2e)$ is the flux quantum.

The resonator modes a_n and a_{n+1} couple inductively to the top loop of B_n (see Fig. 1). The total magnetic flux in the top loop is given by

$$\phi_n^t = \pi \cos(\omega_0 t) + \phi_{n,\text{res}}, \quad (3)$$

where the first term is the flux from an external ac drive (with amplitude π and frequency ω_0), while the second one

$$\phi_{n,\text{res}} = \theta_{n,n+1}(a_{n+1} + a_{n+1}^\dagger) - \theta_{n,n}(a_n + a_n^\dagger) \quad (4)$$

is the flux from the resonator modes. The coupling constants $\theta_{n,n'}$ quantify the contribution of the resonator modes $a_{n'}$ to the connecting circuit B_n . The sign of $\theta_{n,n+1}$ can be designed to be either the same or opposite to that of $\theta_{n,n}$, depending on the geometry of the qubit-resonator coupling. Here we choose $\theta_{n,n+1} = \theta_{n,n} \equiv \delta\theta$. In terms of the resonator parameters, $\delta\theta$ is given by⁵¹

$$\delta\theta = \frac{2e}{\hbar} \frac{A_{\text{eff}}}{d_0 c} \sqrt{\frac{\hbar\omega_c}{C_0}}, \quad (5)$$

where A_{eff} is an effective coupling area, C_0 the capacitance of the resonator, and d_0 the effective spacing in the resonator. In writing Eqs. (4) and (5), we assumed that the magnitudes of fluxes from all resonators are equal and that the signs of the fluxes from adjacent resonators are opposite to each other.

The flux ϕ_n^b in the bottom loop includes an external ac driving and a tunable dc flux ϕ_{b0} :

$$\phi_n^b = -\frac{\pi}{2} \cos(\omega_0 t) + \phi_{b0}. \quad (6)$$

Note that the ac part of ϕ_n^b has the same frequency, but opposite sign of its amplitude compared to the ac part of ϕ_n^t . We choose these amplitudes so that the phase drops φ_n^3 on the bottom junctions do not have an explicit time dependence. This is one of the crucial ingredients in the derivation of the effective Hamiltonian in Sec. II B.

The ac magnetic fluxes in this simulator can be realized by fabricating control wires that couple both to the top- and bottom loops, and applying a microwave pump to the wires. At the same time, the dc magnetic flux in the bottom loops can be implemented by applying a dc current to a separate control wire designed near those loops. Such an implementation should ensure that no significant dc bias couples to the top loops. It should also be emphasized that the only tunable parameters in this circuit are the dc bias ϕ_{b0} and the frequency of the ac drive ω_0 .

By generalizing the standard expression for the effective Josephson energy of a SQUID loop (with two junctions, threaded by a magnetic flux)⁵², the total Josephson energy of the connecting circuit B_n can be written as

$$H_n^J = -\sum_{i=1}^3 E_J^i \cos \varphi_n^i, \quad (7)$$

where E_J^i are the Josephson energies of the three junctions. We will hereafter assume that $E_J^1 = E_J^2 \equiv E_J$ and $E_J^3 = E_{Jb}$.

B. Effective Hamiltonian in the rotating frame of the drive

Given the explicit time dependence originating from the driving terms, we resort to studying this system in

the rotating frame of the drive, i.e., adopt the interaction picture defined by a reference Hamiltonian

$$H_0 = \hbar\omega_0 \sum_n a_n^\dagger a_n. \quad (8)$$

The system dynamics in this rotating frame are described by the Hamiltonian

$$H_I = e^{\frac{i}{\hbar}H_0 t} \left[\sum_n (H_n^s + H_n^J) - H_0 \right] e^{-\frac{i}{\hbar}H_0 t}, \quad (9)$$

which can be recast as

$$H_I = \sum_n \left(\hbar\delta\omega a_n^\dagger a_n + \frac{E_z}{2} \sigma_n^z \right) + e^{\frac{i}{\hbar}H_0 t} \sum_n H_n^J e^{-\frac{i}{\hbar}H_0 t}, \quad (10)$$

with $\delta\omega \equiv \omega_c - \omega_0$. The explicit form of the Josephson-coupling term H_n^J in the rotating frame is derived in detail in Appendix A. Its time-independent part is given by

$$\bar{H}_n^J = -2 \left[t_r - \frac{1}{2} E_J J_1(\pi/2) \phi_{n,\text{res}} \right] \cos(\varphi_n - \varphi_{n+1}), \quad (11)$$

where $J_n(x)$ are Bessel functions of the first kind, and

$$t_r = E_J J_0(\pi/2) (1 + \cos \phi_{b0}) \quad (12)$$

is determined by the Josephson energy of the bottom junction, which, for convenience, is chosen as $E_{Jb} = 2E_J J_0(\pi/2)$. Along with the first two terms in Eq. (10), the time-independent part $\sum_n \bar{H}_n^J$ of the Josephson-coupling term forms the effective Hamiltonian of the system in the rotating frame. Namely, the remaining (time-dependent) part of this transformed Josephson-coupling term can be neglected due to its rapidly-oscillating character (for details, see Appendix A), in accordance with the rotating-wave approximation (RWA).

By expanding $\cos(\varphi_n - \varphi_{n+1})$ to quadratic order in the phase difference $\varphi_n - \varphi_{n+1}$ and defining pseudospin-1/2 operators σ_n that correspond to the lowest two eigenstates of the transmon, we find that

$$\begin{aligned} -2 \cos(\varphi_n - \varphi_{n+1}) &\approx -2 + 4\delta\varphi_0^2 \\ &- 2\delta\varphi_0^2 \left(\sigma_n^+ \sigma_{n+1}^- + \sigma_n^- \sigma_{n+1}^+ - \frac{\sigma_n^z + \sigma_{n+1}^z}{2} \right). \end{aligned} \quad (13)$$

Here $\delta\varphi_0^2 \equiv (2E_{C1}/E_{J1})^{1/2}$ is the quantum displacement of the gauge-invariant phase (E_{C1} and E_{J1} are the charging- and Josephson energies of an individual transmon, respectively); for a typical transmon ($E_{J1}/E_{C1} \sim 100$), we have $\delta\varphi_0^2 \approx 0.15$. Note that the above expansion in powers of $\varphi_n - \varphi_{n+1}$ is justified not only by the smallness of this phase difference in the regime of interest for transmons ($E_{J1} \gg E_{C1}$), but also by the rapidly vanishing coefficients in the expansion (proportional to higher powers of $\delta\varphi_0^2$). The full expression for \bar{H}_n^J (not shown

here) can easily be obtained by combining Eqs. (11) and (13).

It should be stressed that in writing Eq. (13) we have omitted the terms $\sigma_n^- \sigma_{n+1}^- + \sigma_n^+ \sigma_{n+1}^+$. Even in the most general (multilevel) treatment of transmons, such terms are conventionally neglected by virtue of the RWA.

We now switch to the spinless-fermion representation of the pseudospin-1/2 operators via the Jordan-Wigner transformation

$$1 + \sigma_n^z \rightarrow 2c_n^\dagger c_n, \quad \sigma_n^+ \sigma_{n+1}^- + \sigma_n^- \sigma_{n+1}^+ \rightarrow c_n^\dagger c_{n+1} + \text{h.c.} \quad (14)$$

The effective Hamiltonian of the system in the rotating frame

$$H_{\text{eff}} = H_{\text{ph}} + H_e + H_{e\text{-ph}} \quad (15)$$

includes the free-phonon term with the effective phonon frequency $\delta\omega$,

$$H_{\text{ph}} = \hbar\delta\omega \sum_n a_n^\dagger a_n, \quad (16)$$

the (spinless-fermion) excitation hopping term

$$H_e = -t_0 \sum_n (c_n^\dagger c_{n+1} + \text{h.c.}), \quad (17)$$

with $t_0 \equiv 2\delta\varphi_0^2 t_r$ being the effective bare hopping energy, and the excitation-phonon coupling term $H_{e\text{-ph}}$ whose explicit form will be specified shortly. Note that, strictly speaking, H_e also contains the diagonal (on-site energy) terms $c_n^\dagger c_n$ for spinless fermions, originating from the σ_n^z terms in Eqs. (1) and (13). Yet, in consistency with the usual practice in studying coupled e-ph models, we hereafter disregard them as they only represent a constant band offset for our itinerant fermionic excitations.

The coupling Hamiltonian $H_{e\text{-ph}}$ consists of two contributions: the SSH term

$$\begin{aligned} H_{\text{SSH}} &= g\hbar\delta\omega \sum_n (c_n^\dagger c_{n+1} + \text{h.c.}) \\ &\times \left[(a_{n+1} + a_{n+1}^\dagger) - (a_n + a_n^\dagger) \right], \end{aligned} \quad (18)$$

and the BM term

$$\begin{aligned} H_{\text{BM}} &= -g\hbar\delta\omega \sum_n c_n^\dagger c_n \\ &\times \left[(a_{n+1} + a_{n+1}^\dagger) - (a_{n-1} + a_{n-1}^\dagger) \right], \end{aligned} \quad (19)$$

where the dimensionless coupling strength g is defined by the relation

$$g\hbar\delta\omega = \delta\varphi_0^2 E_J J_1(\pi/2) \delta\theta. \quad (20)$$

The SSH term physically accounts for the dynamical dependence of the hopping integral (i.e., the excitation bandwidth) on the phonon displacements $u_n \propto a_n + a_n^\dagger$, to first order in these displacements; it is nonlocal in that

the hopping integral between sites n and $n+1$ depends on the displacements on both sites¹⁹. The BM term, on the other hand, also describes a nonlocal e-ph interaction; it accounts for the antisymmetric coupling of the excitation density at site n with the phonon displacements on the neighboring sites $n-1$ and $n+1$. Being an example of a “density-displacement” type coupling, it can be viewed as a nonlocal generalization of the Holstein-type e-ph interaction.

It is worthwhile to mention that an example of a real electronic system where both e-ph coupling mechanisms discussed here play important roles is furnished by the cuprates. In those materials, both mechanisms involve the planar Cu-O bond-stretching phonon modes, also known as breathing modes. These bond-stretching modes couple to electrons both via a direct modulation of the hopping integral (SSH-type coupling)⁵³, and through electrostatic changes in the Madelung energies that originate from displacements of orbitals (BM-type coupling)^{54,55}.

C. Relevant parameter range

A suitable set of parameters for the SC resonators is given by $d_0 = 25 \mu\text{m}$, $A_{\text{eff}} = 100 \mu\text{m}^2$, $C_0 = 2 \text{ fF}$, $\omega_c/2\pi = 24 \text{ GHz}$, while the effective phonon frequency can be $\delta\omega/2\pi = 200 \text{ MHz}$ or 300 MHz . In addition, we choose E_J for the Josephson junctions in the connecting circuits such that $2\delta\varphi_0^2 E_J/2\pi\hbar = 200 \text{ GHz}$. From this choice of parameter values, it follows that $\delta\theta = 3.5 \times 10^{-3}$ and $g\delta\omega/2\pi = 198 \text{ MHz}$.

The hopping integral t_0 can be adjusted in-situ by varying the dc magnetic flux ϕ_{b0} between the bottom two junctions. This is illustrated in Fig. 2(a), where the ratio $t_0/\hbar\delta\omega$ is shown for ϕ_{b0}/π between 0.95 and 0.99. For the chosen values of ϕ_{b0}/π we are mainly in the adiabatic regime ($t_0 > \hbar\delta\omega$), entering the antiadiabatic regime ($t_0 < \hbar\delta\omega$) for $\phi_{b0}/\pi \approx 0.98$. For the same range of values for ϕ_{b0} , the effective coupling strength

$$\lambda = 2g^2 \frac{\hbar\delta\omega}{t_0} \quad (21)$$

varies from the weak-coupling to the strong-coupling regime, as can be inferred from Fig. 2(b). For instance, with $\delta\omega/2\pi = 200 \text{ MHz}$ and $\phi_{b0}/\pi = 0.95$, we have $\lambda = 0.34$; for the same value of $\delta\omega$, $\phi_{b0}/2\pi = 0.98$ yields $\lambda = 2.1$.

III. SMALL-POLARON SIGNATURES AND SHARP TRANSITION

The eigenstates of our effective single-particle Hamiltonian H_{eff} are the joint eigenstates of H_{eff} and the total quasimomentum operator $K_{\text{tot}} = \sum_k k c_k^\dagger c_k + \sum_q q a_q^\dagger a_q$, where c_k and a_q are the excitation- and phonon annihilation operators in momentum space. For conve-

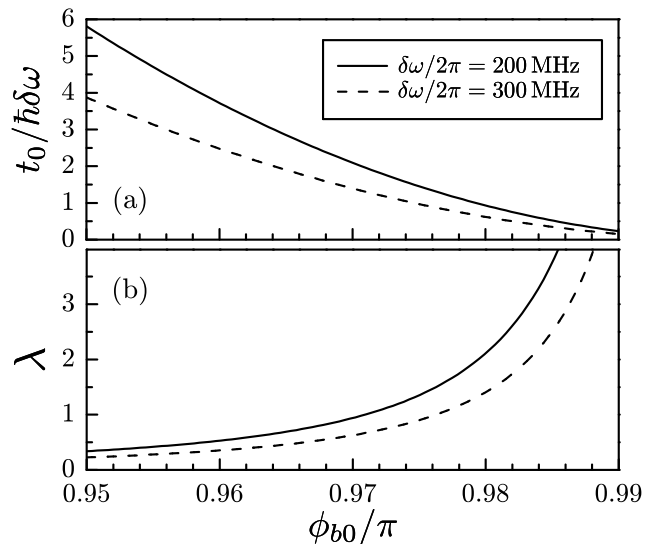


Figure 2: Dimensionless parameters of the simulator: (a) Ratio of the hopping integral and the phonon energy, and (b) effective coupling strength λ , both shown as a function of the tunable dc-flux ϕ_{b0} , for two different values of the effective phonon frequency $\delta\omega$.

nience, we will express quasimomenta in units of the inverse lattice period, so that $c_k = N^{-1/2} \sum_n e^{ikn} c_n$ and $a_q = N^{-1/2} \sum_n e^{iqn} a_n$. The eigenvalues of the operator K_{tot} will hereafter be denoted as K . In particular, K_{gs} will stand for the quasimomentum corresponding to the ground state of the system (i.e., the dispersion minimum of the effective, dressed-excitation Bloch band).

A. Momentum dependence of the resulting e-ph coupling

Before embarking on a numerical calculation of the ground state of the system, it is worthwhile to analyze the momentum dependence of the vertex function corresponding to the resulting e-ph coupling term:

$$H_{\text{e-ph}} = N^{-1/2} \sum_{k,q} \gamma(k,q) c_{k+q}^\dagger c_k (a_{-q}^\dagger + a_q). \quad (22)$$

This vertex function

$$\gamma(k,q) = 2ig\hbar\delta\omega \left[\sin k + \sin q - \sin(k+q) \right] \quad (23)$$

consists of the k - and q -dependent SSH part $\gamma_{\text{SSH}}(k,q) = 2ig\hbar\delta\omega [\sin k - \sin(k+q)]$, and the BM part $\gamma_{\text{BM}}(q) = 2ig\hbar\delta\omega \sin q$ that only features q dependence. Since the overall vertex function $\gamma(k,q)$ depends on both k and q , it does not belong to the domain of applicability of the Gerlach-Löwen theorem²³, which rules out a nonanalytic behavior of the single-particle quantities. While k - and q -dependent couplings do not necessarily lead to nonanalyticities⁵⁶, such nonanalyticity indeed occurs

in a model with the pure SSH coupling [vertex function $\gamma_{\text{SSH}}(k, q)$]⁵⁷. In the following (see Sec. III C), we show that the model with combined SSH and BM couplings studied here displays a similar sharp transition between a quasifree excitation and a small polaron.

B. Details of exact diagonalization

To determine the ground-state properties of our resulting coupled e-ph model, we employ the conventional Lanczos diagonalization⁵⁸ in combination with a controlled truncation of the phonon Hilbert space.

The Hilbert space of the system is spanned by states given as direct products $|n\rangle_e \otimes |\mathbf{m}\rangle_{\text{ph}}$. Here, $|n\rangle_e = c_n^\dagger |0\rangle_e$ is the state of the excitation localized at the site n , $\mathbf{m} = (m_1, \dots, m_N)$ are the phonon occupation numbers, and $|\mathbf{m}\rangle_{\text{ph}} = \prod_{i=1}^N (1/\sqrt{m_i!}) (b_i^\dagger)^{m_i} |0\rangle_{\text{ph}}$. Restricting ourselves to a truncated phonon Hilbert space that includes states with at most M phonons (total number on a lattice with N sites), we take into account all m -phonon states with $0 \leq m_i \leq m$, where $m = \sum_{i=1}^N m_i \leq M$. The dimension of the total Hilbert space is $D = D_e \times D_{\text{ph}}$, where $D_e = N$ and $D_{\text{ph}} = (M + N)! / (M! N!)$.

To further reduce the dimension of the Hamiltonian matrix to be diagonalized, we exploit the discrete translational invariance of our finite system, mathematically expressed as the commutation $[H_{\text{eff}}, K_{\text{tot}}] = 0$ of the Hamiltonian H_{eff} and the total quasimomentum operator K_{tot} . This allows us to perform diagonalization of H_{eff} in sectors corresponding to the eigensubspaces of K_{tot} . For that to accomplish, we make use of the symmetrized basis

$$|K, \mathbf{m}\rangle = N^{-1/2} \sum_{n=1}^N e^{iKn} T_n(|1\rangle_e \otimes |\mathbf{m}\rangle_{\text{ph}}), \quad (24)$$

where T_n denotes (discrete) translation operators. Thus, the dimension of each K -sector of the total Hilbert space is $D_K = D_{\text{ph}}$.

Following an established phonon Hilbert-space truncation procedure⁵⁹, the system size (N) and the maximum number of phonons retained (M) are increased until the convergence for the ground-state energy $E_{\text{gs}}^{(M)}$ and the phonon distribution is reached. Our adopted convergence criterion is that the relative error in the ground-state energy and the phonon distribution upon further increase of N and M is not larger than 10^{-4} . While for the momentum-independent (completely local in real space) Holstein coupling the system size is essentially inconsequential, for nonlocal couplings of the kind studied here this is not the case. In particular, the adopted quantitative convergence criterion is satisfied for the system size $N = 10$ (with periodic boundary conditions) and requires the total of $M = 8$ phonons.

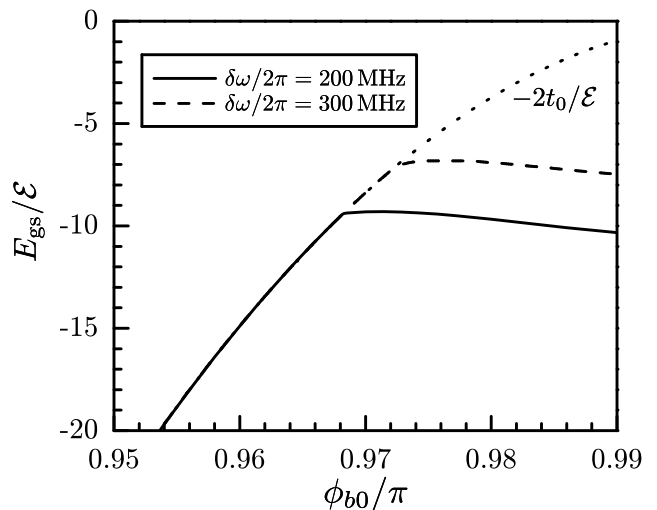


Figure 3: Ground-state energy, expressed in units of $\mathcal{E} \equiv 10^{-3} \delta\varphi_0^2 E_J = 2\pi\hbar \times 100$ MHz, as a function of the experimentally-tunable parameter ϕ_{b0} . The solid curve corresponds to the effective phonon frequency $\delta\omega/2\pi = 200$ MHz, while the dashed curve corresponds to $\delta\omega/2\pi = 300$ MHz.

C. Results and Discussion

We now discuss the results obtained by exact diagonalization of our effective model. Unlike more conventional situation, in which the effective coupling strength λ [cf. Eq. (21)] is changed by varying the dimensionless coupling constant g (for fixed ratio of the relevant hopping integral and the phonon energy)⁸, here we work with a fixed value of $g\delta\omega$ [recall Eq. (20)]. We effectively change λ by varying the bare hopping integral t_0 through the experimentally-tunable parameter ϕ_{b0} , in accordance with Eq. (12).

Our main finding is that at a critical value of ϕ_b (i.e., of the effective coupling strength λ), there is a sharp transition (nonanalyticity) of all relevant quantities⁵⁷. This transition originates from a (real) level crossing and is of first order. It is illustrated in Fig. 3, where the ground-state energy (expressed in units of $\mathcal{E} \equiv 10^{-3} \delta\varphi_0^2 E_J = 2\pi\hbar \times 100$ MHz) is shown as a function of ϕ_{b0} . The sharp transition physically corresponds to a change – at a critical value of ϕ_{b0} – from a non-degenerate ground state that corresponds to the zero quasimomentum ($K_{\text{gs}} = 0$), to a twofold-degenerate one corresponding to equal and opposite (nonzero) quasimomenta K_{gs} and $-K_{\text{gs}}$. For $\delta\omega/2\pi = 200$ MHz this critical value is $(\phi_{b0})_c \approx 0.968\pi$, while for $\delta\omega/2\pi = 300$ MHz we find $(\phi_{b0})_c \approx 0.972\pi$. The corresponding critical values of the effective coupling strength are $\lambda_c \approx 0.83$ and 0.72 , respectively. Shown in Fig. 4 are two small-polaron Bloch-band dispersions throughout the Brillouin zone (for $\delta\omega/2\pi = 200$ MHz and two different values of ϕ_{b0}), both with band minima (ground states) at nonzero quasimomenta.

For sufficiently strong coupling – e.g., $\phi_{b0} \gtrsim 0.98$ for $\delta\omega/2\pi = 200$ MHz – the quasimomentum K_{gs} corre-

sponding to the single-particle ground state saturates at around $\pi/2$ (see the dash-dotted curve in Fig. 4). It should be stressed that – while the ground-state undergoes a sharp transition – the quasimomentum K_{gs} itself varies smoothly between $K_{\text{gs}} = 0$ and this saturation value as ϕ_{b0} is increased beyond its critical value.

Apart from the occurrence of a sharp transition, another interesting aspect of our findings is an effective “compensation” of SSH and BM couplings below the critical value of ϕ_{b0} . This is indicated in Fig. 3, where the ground-state energy curve essentially follows the bare-dispersion curve $E = -2t_0(\phi_{b0})$ all the way up to the critical value of ϕ_{b0} . This peculiar effect can be ascribed to the character of the resulting momentum dependence of the e-ph vertex function in Eq. (23), being a consequence of the fact that here the SSH and BM coupling strengths are the same¹⁹. This phenomenon could have profound consequences for transport properties of real electronic systems with competing SSH and BM couplings.

The central quantity for characterizing the small-polaron regime is the quasiparticle residue $Z_k \equiv |\langle \Psi_k | \psi_k \rangle|^2$, i.e., the module squared of the overlap between the bare-excitation Bloch state $|\Psi_k\rangle \equiv c_k^\dagger |0\rangle$ and the (dressed) Bloch state $|\psi_k\rangle$ of the coupled e-ph system that corresponds to the same quasimomentum ($K = k$). In particular, having determined the ground-state wave function $|\psi_{\text{gs}}\rangle \equiv |\psi_{K=K_{\text{gs}}}\rangle$ we can compute $Z_{\text{gs}} \equiv Z_{k=K_{\text{gs}}}$, a quantity characterizing the ground state of the system. While $Z_{\text{gs}} \approx 1$ indicates the weak-coupling regime (quasifree excitation), its reduced values in the strong-coupling regime [see Fig. 5(a)] signify the presence of small polarons, with these two regimes being separated by a nonanalyticity at the critical value of ϕ_{b0} . It is interesting to note that, unlike for the Holstein model where $Z_{\text{gs}} \approx 0$ for strong enough coupling, here

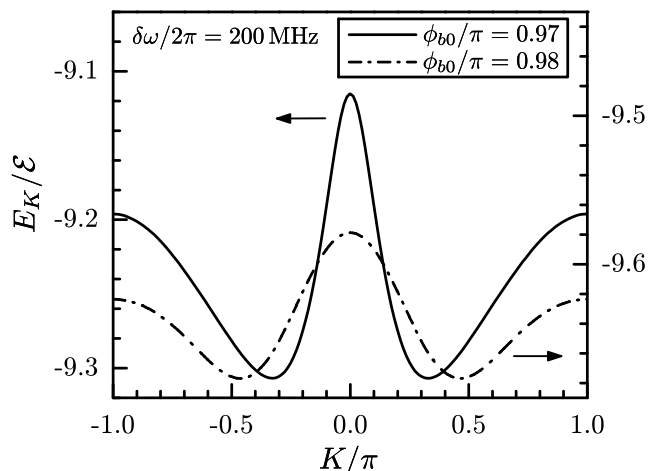


Figure 4: Small-polaron Bloch dispersions for two different values of the tunable parameter ϕ_{b0} , shown throughout the Brillouin zone. The solid curve corresponds to the y -axis scale marked on the left, while the dash-dotted curve corresponds to the scale on the right, as indicated by the arrows.

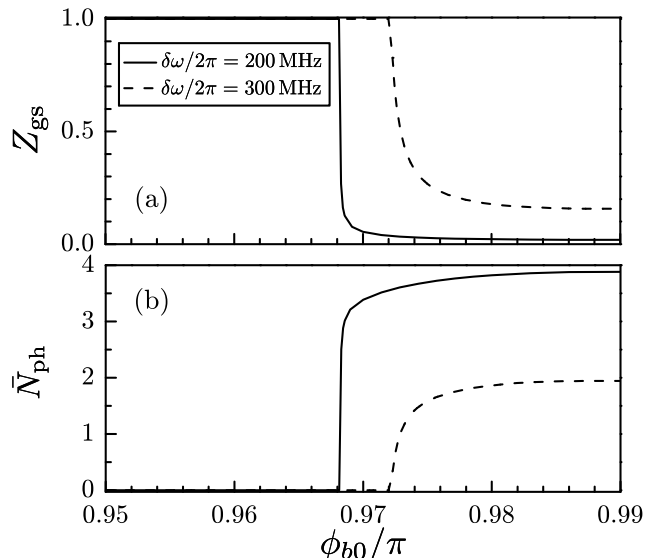


Figure 5: Characterization of the sharp transition between a quasifree excitation and a small polaron: (a) Ground-state quasiparticle residue $Z_{\text{gs}} \equiv Z_{k=K_{\text{gs}}}$, and (b) average number of phonons \bar{N}_{ph} , versus the experimentally-tunable parameter ϕ_{b0} . The solid and dashed curves correspond to $\delta\omega/2\pi = 200$ MHz and $\delta\omega/2\pi = 300$ MHz, respectively.

Z_{gs} may saturate at a finite value. As can be inferred from Fig. 5(a), for $\delta\omega/2\pi = 300$ MHz we find such saturation at $Z_{\text{gs}} \approx 0.15$.

Another relevant quantity is the average number of phonons in the ground state

$$\bar{N}_{\text{ph}} \equiv \langle \psi_{\text{gs}} | \sum_{n=1}^N a_n^\dagger a_n | \psi_{\text{gs}} \rangle. \quad (25)$$

The change of this quantity from values close to zero [see Fig. 5(b)] to a nonzero value $\bar{N}_{\text{ph}} \gtrsim 3$ marks the transition from a quasifree excitation to a small polaron. The aforementioned effective compensation of the SSH and BM couplings below $(\phi_{b0})_c$ is reflected in the vanishing phonon-dressing of fermionic excitations, the flat parts of the curves in Fig. 5(b).

The average phonon number \bar{N}_{ph} is amenable to a direct measurement in our system, through measurements of photon numbers on different resonators (see Sec. IV B). Likewise, the second moment of the effective phonon distribution can also be extracted by measuring the photon squeezing in the resonators^{10,60}. More generally, the complex multiphononic nature of small-polaron excitations can be fully captured by computing the entire phonon distribution, which is depicted in Fig. 6 for both values of the effective phonon frequency $\delta\omega$ used above. While for $\delta\omega/2\pi = 200$ MHz the distribution has a broad maximum at $N_{\text{ph}} \approx 4$, the one for $\delta\omega/2\pi = 300$ MHz – corresponding to a smaller effective coupling strength λ [cf. Eqs. (20) and (21)] – has a weakly-pronounced maximum at around $N_{\text{ph}} \approx 1$. By contrast, the dotted curve

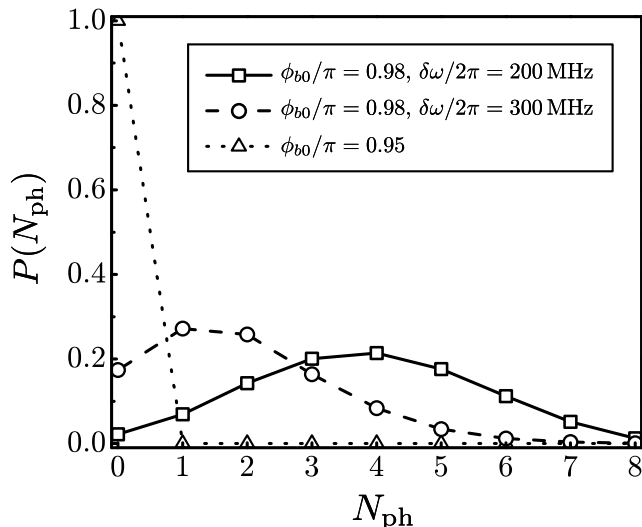


Figure 6: Illustration of the multiphononic nature of small-polaron excitations: Full ground-state phonon distribution at $\phi_{b0}/\pi = 0.98$, for $\delta\omega/2\pi = 200$ MHz (squares) and $\delta\omega/2\pi = 300$ MHz (circles). The dotted curve corresponds to the phonon distribution for $\phi_{b0}/\pi = 0.95$, i.e., below the critical coupling strength.

in Fig. 6, representing a typical phonon distribution for couplings below the critical one, is very strongly peaked at $N_{\text{ph}} = 0$.

While phonon distributions peaked at zero phonons are characteristic of all small-polaron models in the weak-coupling regime (e.g., below the onset of the polaron crossover in the Holstein model), the peculiarity of our findings is that here such distribution persists all the way up to the critical coupling strength. Although the sharp transitions of the type found here do not result from any kind of cooperative behavior (as is typical for quantum phase transitions in many-particle systems), the observed peculiar behavior allows us to treat \bar{N}_{ph} as an effective “order parameter” for the predicted sharp transition. Given that \bar{N}_{ph} is a directly measurable quantity in our system, this fact will facilitate experimental verification of the existence of this transition.

IV. STATE PREPARATION, DETECTION, AND ROBUSTNESS

A. State-preparation protocol

The feasibility of our simulation scheme is contingent upon the ability to prepare the desired small-polaron Bloch states. For this purpose, we make use of the state-preparation protocol proposed in our previous work (Ref. 10), which is only briefly explained in the following.

We assume that the initial state of the system is the vacuum state $|G_0\rangle \equiv |0\rangle_e \otimes |0\rangle_{\text{ph}}$. This state, with no excitations (i.e., with all qubits in their spin-down states)

and all resonators in their respective vacuum states, can be prepared via thermalization in a low-temperature environment. Our target state is the dressed-excitation (in the special case, small polaron) Bloch state $|\psi_K\rangle$, corresponding to the eigenvalue K of the total quasimomentum operator K_{tot} .

The microwave driving required for preparing this state is envisioned to be of the form

$$\Omega_q(t) = \frac{\hbar\beta(t)}{\sqrt{N}} \sum_n (\sigma_n^+ e^{-iqn} + \sigma_n^- e^{iqn}), \quad (26)$$

where $\beta(t)$ describes its time dependence, and the phase factors $e^{\pm iqn}$ indicate that spin-flip operations are applied to different qubits with a q -dependent phase difference. It is easy to show that the transition matrix element of the operator $\Omega_q(t)$ between the states $|G_0\rangle$ and $|\psi_K\rangle$ is given by¹⁰

$$|\langle\psi_K|\Omega_q(t)|G_0\rangle| = \hbar|\beta(t)|\sqrt{Z_K}\delta_{q,K}. \quad (27)$$

Assuming that $\beta(t) = 2\beta_p \cos(\omega_K t)$, where $\hbar\omega_K$ is the energy difference between the states $|G_0\rangle$ and $|\psi_K\rangle$, in the RWA the two states are Rabi-coupled with the effective Rabi frequency $\beta_p\sqrt{Z_K}$. Thus, starting from the vacuum state $|G_0\rangle$, the state $|\psi_K\rangle$ will be prepared within a time interval of duration¹⁰

$$\tau_{\text{prep}} = \frac{\pi\hbar}{2\beta_p\sqrt{Z_K}}. \quad (28)$$

The form of the last expression is consistent with the expectation that the more strongly-dressed states (smaller Z_K) require longer preparation times. For the small-polaron ground states with $K = \pm K_{\text{gs}}$ these preparation times are much shorter than the decoherence time T_2 . For instance, assuming that the pumping amplitude is $\beta_p/(2\pi\hbar) = 40$ MHz and taking the values for Z_{gs} at the onset of the small-polaron regime [see Fig. 5(a)], we respectively find that $\tau_{\text{prep}} \approx 24$ ns for $\delta\omega/2\pi = 200$ MHz, and $\tau_{\text{prep}} \approx 17$ ns for $\delta\omega/2\pi = 300$ MHz. The obtained state-preparation times are three orders of magnitude shorter than currently achievable decoherence times $T_2 \sim 20 - 100$ μs of transmon qubits^{33,34}, this being a strong indication of the feasibility of our proposed protocol.

The above Rabi-coupling state-preparation protocol, which ensures energy and momentum conservation¹⁰, can in principle be adapted to other systems by taking into account their underlying symmetries. Importantly, the ultimate success of this scheme in different systems will depend on the character of their underlying absorption spectra, as described by the corresponding spectral functions (see Sec. V C). As far as our system is concerned, it should be stressed that the absorption spectra of electronic systems coupled with optical phonons (i.e., phonon modes with a gap in their spectrum) are characterized by generic spectral functions in which the “coherent” part (with a finite spectral weight) is energetically well separated from the incoherent background^{12,61}. This form of

absorption spectra should here allow one to avoid inadvertent population of other (excited) states while preparing a desired small-polaron ground state of the system.

B. Experimental detection

Here we discuss the method for measuring the average phonon number \bar{N}_{ph} [cf. Eq. (25)], a quantity which can be thought of as an order parameter for the sharp small-polaron transition (cf. Sec. III C). As already stressed above, in our implementation \bar{N}_{ph} corresponds to the average total photon number on the resonators. Owing to the discrete translational symmetry of the system, the measurement of \bar{N}_{ph} can be reduced to the measurement of the mean photon number of one of the resonators. This can be accomplished by adding an ancilla qubit which couples to this particular resonator¹⁰, but only during the measurement; this qubit is assumed to be far-detuned from the resonator modes. By measuring the qubit state, the mean photon number on this resonator can be extracted, which multiplied with the total system size N yields the result for \bar{N}_{ph} .

C. Robustness of the simulator

As in every other quantum-computation device, decoherence effects should also be present in our simulator. Possible excitations in this system correspond either to flipping of the qubit states or to displacement of the resonator modes, which are subject to the decoherence of the qubits and resonators. In addition to very long dephasing times ($T_2 \sim 20 - 100 \mu\text{s}$) of transmon qubits achieved in recent years, for coplanar waveguide resonators the damping time of the microwave photons can reach the same order of magnitude as T_2 , with a quality factor larger than 10^6 . The relevant energy scales in our simulator (effective phonon frequency, e-ph coupling strength, and hopping energy) are all of the order of 100 MHz, far exceeding the decoherence rates. Besides, as shown in Sec. IV A, even for very strongly-dressed polaron states the typical duration of the state-preparation protocol is three orders of magnitude smaller than the decoherence times. Finally, in the low-temperature environment of our system thermal excitations – which here have energies of a few GHz – can be safely neglected.

The pump pulses of the kind described in Sec. IV A may, in principle, induce unwanted transitions (leakage) to higher energy levels in a transmon qubit⁶². Namely, in all qubits based on weakly-anharmonic oscillators leakage from the two-dimensional qubit Hilbert space (computational states) is the leading source of errors at short pulse times⁶³. This is especially pronounced if the pulse bandwidth is comparable to the anharmonicity. However, in a typical transmon with $E_{J1}/E_{C1} \sim 50 - 100$ and a negative anharmonicity of $\sim 3 - 5\%$, even pulses with durations of only a few ns are sufficiently frequency se-

lective that the unwanted transitions can be neglected²⁸. In our system, there is an off resonance of around 500 MHz for such transitions. For a typical driving amplitude $\beta_p/2\pi \approx 40$ MHz, the probability of leakage is below one percent, which is a reasonable error rate for the simulator.

Fabrication-related variations in the parameters of Josephson junctions, which are $1 - 2\%$ at best and typically up to 5% , are unavoidable even in modern-day SC circuits. This is, however, not expected to jeopardize the observation of the predicted nonanalytic behavior in our system. Namely, as is known from general polaron theory (e.g., the Gerlach-Löwen theorem) the presence of such nonanalyticities (or, more often, the absence thereof) in a particular coupled e-ph model is intimately related to the type of the momentum dependence of the resulting coupling. This momentum dependence, in its own right, depends on the character of the particular coupling mechanisms involved (recall discussions in the introduction and Sec. III A), rather than on quantitative details such as the magnitude of the bare hopping integral (which in our case is determined by E_J). Thus the occurrence of the real level crossing which gives rise to the sharp feature in the ground-state energy of the system should be quite robust; the small variations in parameters such as E_J can only lead to a slight shift of the critical coupling strength at which this crossing takes place. That this shift is expected to be small – for small variations ΔE_J of the Josephson energy ($\Delta E_J/E_J \lesssim 5\%$) – can be inferred from the expression for the effective coupling strength λ [cf. Eq. (21)]. Because $\lambda \propto g^2/t_0$, where both g and t_0 depend linearly on E_J , we have that $\Delta\lambda/\lambda = \Delta E_J/E_J$.

V. EXTRACTING CORRELATION FUNCTIONS USING A RAMSEY SEQUENCE: STUDY OF THE POLARON-FORMATION DYNAMICS

A. Relevant Green's functions

Generally speaking, dynamical response functions – Fourier transforms of retarded two-time Green's functions – provide a natural framework for characterizing excitations in many-body systems. The relevant single-particle retarded two-time Green's function in the problem at hand is given by

$$G_+^{\text{R}}(k, t) = -\frac{i}{\hbar} \theta(t) \langle G_0 | [c_k^\dagger(t), c_k]_+ | G_0 \rangle, \quad (29)$$

where $c_k^\dagger(t)$ is a single-particle operator in the Heisenberg representation and $[\dots]_+$ stands for an anticommutator. More explicitly, $c_k(t) = U_H^\dagger(t) c_k U_H(t)$, where $U_H(t)$ is the time-evolution operator corresponding to the lab-frame counterpart $H = H(t)$ of our effective Hamiltonian H_{eff} in the rotating frame. The explicit forms of H and U_H are not relevant for our present purposes. In fact, the only relevant property of the Hamiltonian H is

that its symmetries in the spinless-fermion (pseudospin) sector of the problem are the same as those of the Hamiltonian H_{eff} , since this part of H_{eff} preserves its form in the interaction picture.

It should be emphasized that, while the natural Green's functions for spinless fermions are those that involve anticommutators [cf. Eq. (29)], in the single-particle problem at hand the commutator Green's function

$$G_-^{\text{R}}(k, t) = -\frac{i}{\hbar} \theta(t) \langle G_0 | [c_k^\dagger(t), c_k]_- | G_0 \rangle. \quad (30)$$

contains the same physical information. Namely, given that $|G_0\rangle$ is a vacuum state, we have that $c_k^\dagger(t)c_k|G_0\rangle = 0$, which implies that in this special case $G_-^{\text{R}}(k, t) = -G_+^{\text{R}}(k, t)$.

Anticipating the use of a real-space experimental probe (see Sec. V B), we further note that the last momentum-space Green's function can be retrieved from the real-space resolved ones, i.e.,

$$G_-^{\text{R}}(k, t) = N^{-1} \sum_{n, n'} e^{ik \cdot (n-n')} G_{nn'}^{\text{R}}(t), \quad (31)$$

where $G_{nn'}^{\text{R}}(t) \equiv -(i/\hbar)\theta(t)\langle G_0 | [c_n^\dagger(t), c_{n'}]_- | G_0 \rangle$. By switching to the pseudospin-1/2 operators and taking into account that the Jordan-Wigner string operators act trivially on the ground state $|G_0\rangle$, these real-space commutator Green's function can be rewritten as

$$G_{nn'}^{\text{R}}(t) = -\frac{i}{\hbar} \theta(t) \langle G_0 | [\sigma_n^+(t), \sigma_{n'}^-]_- | G_0 \rangle. \quad (32)$$

They can further be transformed to the form

$$G_{nn'}^{\text{R}}(t) = \mathcal{G}_{nn'}^{xx} + \mathcal{G}_{nn'}^{yy} - i(\mathcal{G}_{nn'}^{xy} - \mathcal{G}_{nn'}^{yx}), \quad (33)$$

where

$$\mathcal{G}_{nn'}^{\alpha\beta} \equiv -\frac{i}{\hbar} \theta(t) \langle G_0 | [\sigma_n^\alpha(t), \sigma_{n'}^\beta]_- | G_0 \rangle \quad (\alpha, \beta = x, y) \quad (34)$$

and, for simplicity, we suppressed the time argument and the superscript R in the notation for these Green's functions.

B. Many-body Ramsey interference protocol

The Ramsey-interference protocol is in principle applicable in any system where single-site addressability is available and yields naturally the real-space and time-resolved commutator Green's functions of spin operators^{64,65}. In the problem at hand it involves the pseudospin degree of freedom of the transmon qubits.

The general Rabi pulses can be parameterized as

$$R_n(\theta, \phi) \equiv \mathbb{1}_{2 \times 2} \cos \frac{\theta}{2} + i(\sigma_n^x \cos \phi - \sigma_n^y \sin \phi) \sin \frac{\theta}{2}, \quad (35)$$

where $\theta = \Omega\tau$, with Ω being the Rabi frequency and τ the pulse duration; ϕ is the phase of the laser field. The Ramsey protocol makes use of the special case $R_n(\phi) \equiv R_n(\theta = \pi/2, \phi)$ of such pulses, with $\theta = \pi/2$ and arbitrary ϕ .

Quite generally, the Ramsey-interference protocol entails the following steps: (1) perform local $\pi/2$ -rotation at site n (with $\phi = \phi_1$); (2) evolve the system during time t ; (3) perform local $\pi/2$ -rotation at site n' , or global $\pi/2$ -rotation (with $\phi = \phi_2$); (4) measure the system in the σ_z basis at site n' . In our system, the described protocol leads to the measurement result given by the expectation value

$$M_{nn'}(\phi_1, \phi_2, t) = \langle G_0 | R_n^\dagger(\phi_1) U_H^\dagger(t) R_{n'}^\dagger(\phi_2) \sigma_{n'}^z R_{n'}(\phi_2) U_H(t) R_n(\phi_1) | G_0 \rangle. \quad (36)$$

The procedure for extracting relevant Green's function can be simplified by exploiting the symmetries of our system in the pseudospin sector. Since its Hamiltonian involves a sum of an XY -coupling term and σ_n^z terms [recall Eq. (13)], our system has a $U(1)$ symmetry under z -axis pseudospin rotations, implying that $\mathcal{G}_{nn'}^{xx} = \mathcal{G}_{nn'}^{yy}$ and $\mathcal{G}_{nn'}^{xy} + \mathcal{G}_{nn'}^{yx} = 0$. Another symmetry of our system is that under reflections with respect to the z axis ($\sigma_n^x \rightarrow -\sigma_n^x$, $\sigma_n^y \rightarrow -\sigma_n^y$, $\sigma_n^z \rightarrow \sigma_n^z$), which implies that any expectation value involving an odd (total) number of σ_n^x and σ_n^y operators is equal to zero. For a system with these two symmetries, the Ramsey protocol measures⁶⁵

$$M_{nn'}(\phi_1, \phi_2, t) = -\frac{1}{4} [\sin(\phi_1 - \phi_2)(\mathcal{G}_{nn'}^{xx} + \mathcal{G}_{nn'}^{yy}) - \cos(\phi_1 - \phi_2)(\mathcal{G}_{nn'}^{xy} - \mathcal{G}_{nn'}^{yx})]. \quad (37)$$

Thus the combinations $\mathcal{G}_{nn'}^{xx} + \mathcal{G}_{nn'}^{yy}$ and $\mathcal{G}_{nn'}^{xy} - \mathcal{G}_{nn'}^{yx}$ needed to recover $G_{nn'}^{\text{R}}(t)$ [recall Eq. (33)] can be obtained by choosing the angles ϕ_1, ϕ_2 such that $\phi_1 - \phi_2 = \pm\pi/2$ and $\phi_1 = \phi_2$, respectively.

In the realm of SC qubits, the Ramsey-interference protocol is conventionally used to determine the decoherence time T_2 of a single qubit, a procedure known as the Ramsey-fringe experiment³⁴. The use of this protocol is also envisioned for other types of manipulation, such as interaction-free measurements⁶⁶. In the present work, we propose its use on pairs of qubits in a multi-qubit system, for the purpose of extracting the desired two-time correlation- and Green's functions.

C. Spectral function and its relation to the dynamics of small-polaron formation

Provided that the single-particle retarded two-time Green's function [cf. Eq. (29)] is extracted as explained in Secs. V A and V B, we can also obtain the information about the spectral properties of the system. Namely, by Fourier-transforming this Green's function

to momentum-frequency space, the spectral function is obtained as $A(k, \omega) = -(1/\pi)\text{Im} G_+^{\text{R}}(k, \omega)$. The spectral function can quite generally be represented in the form

$$A(k, \omega) = \sum_j |\langle \psi_k^{(j)} | c_k^\dagger | 0 \rangle|^2 \delta(\omega - E_k^{(j)}/\hbar), \quad (38)$$

where $|\psi_k^{(j)}\rangle$ is a complete set of total-quasimomentum k eigenstates of the total Hamiltonian of the coupled e-ph system (in our case H_{eff}), and $E_k^{(j)}$ the corresponding eigenvalues. In the simplest case, the above sum over j includes the polaron-ground state $|\psi_k^{(j=0)}\rangle$ at quasimomentum k and its attendant continuum of states that correspond to the polaron with quasimomentum $k - q$ and an unbound phonon with quasimomentum q . More generally, with increasing coupling strength there will be multiple coherent polaron bands below the one-phonon continuum (threshold for inelastic scattering) which sets in at energy $E_{gs} + \hbar\omega_0$ ⁶¹, where ω_0 is the relevant phonon frequency (in our case $\delta\omega$). All these coherent (split-off from the one-phonon continuum) polaron states contribute to the above sum along with their respective continua.

The spectral function is intimately related to the dynamics of polaron formation. Let us assume that at $t = 0$ a bare-excitation Bloch state with quasimomentum k is prepared and e-ph coupling is turned on (e-ph interaction quench). Then $|\psi(0)\rangle = c_k^\dagger|0\rangle$ is the state of the system at $t = 0$, while at a later time t its state is given by $|\psi(t)\rangle = \sum_j e^{-\frac{i}{\hbar}E_k^{(j)}t} |\psi_k^{(j)}\rangle \langle \psi_k^{(j)} | c_k^\dagger | 0 \rangle$. It is straightforward to verify that by Fourier-transforming the spectral function to the time domain we obtain the amplitude $\langle \psi(t) | c_k^\dagger | 0 \rangle$ to remain in the initial (bare-excitation) state of the system at time t ⁴⁷. The corresponding probability $|\langle \psi(t) | c_k^\dagger | 0 \rangle|^2$ yields the quasiparticle residue at time t , thus describing the dynamics of polaron formation.

In our system, the last procedure can be implemented by making use of the state-preparation protocol described in Sec. IV A to prepare a bare-excitation Bloch state with quasimomentum k and switching on the qubit-resonator coupling at $t = 0$. As a matter of fact, given the character of the polaron formation in our system – where at the critical coupling strength there is an abrupt change from an almost undressed (bare) excitation to a heavily dressed small polaron – a variation of the tunable parameter ϕ_{b0} from slightly below the critical value $(\phi_{b0})_c$ to slightly above this value is essentially equivalent to an e-ph interaction quench. This should be the most straightforward way to implement a quench in our system.

Polaron formation is admittedly a very complex dynamical process even in the case of the momentum-independent e-ph coupling^{46,47}. Even the very fundamental question related to the time it takes to form a polaron, as well as a more detailed understanding of how phonon excitations evolve into the correlated phonon cloud of the polaron quasiparticle, are not fully answered to date. In the presence of strongly-momentum dependent e-ph interactions, which even allow for the occur-

rence of sharp transitions, it should be even more difficult to arrive at a full understanding of this process. Our system, with its unique set of experimental tools, should be very useful in this regard. While the time it takes to form a polaron (after an e-ph interaction quench) should be possible to extract already from measurements of the average phonon number (by measuring the photon number on different resonators), additional characteristics of the polaron-formation dynamics can be unravelled by extracting the spectral function via a Ramsey-interference protocol.

VI. SUMMARY AND CONCLUSIONS

To summarize, we have proposed a superconducting analog quantum simulator for a model with nonlocal electron-phonon couplings of Su-Schrieffer-Heeger and breathing-mode types. The simulator is based on an array of transmon qubits and microwave resonators. In this system, the nearest-neighbor qubits are Josephson-coupled through an appropriately designed connecting circuit, the latter being also inductively coupled to a pair of adjacent resonators. Our setup allows one to simulate the strong excitation-phonon coupling regime, characterized by the small-polaron formation, with quite realistic values of the circuit parameters.

The most interesting feature of the investigated model is the occurrence of a sharp (first-order) transition at a critical coupling strength. This transition results from a real level crossing and physically corresponds to the change from a nondegenerate single-particle ground state at zero quasimomentum ($K_{\text{gs}} = 0$) to a twofold-degenerate one at nonzero quasimomenta K_{gs} and $-K_{\text{gs}}$. Aside from the fact that our suggested setup provides a tunable experimentally platform for observing the sharp transition, what further motivated the present work is the circumstance that e-ph coupling in real materials is insufficiently strong for observing any measurable consequence of this type of transition²⁰.

One of the obvious advantages of superconducting Josephson-junction based systems compared to other quantum-simulation platforms (trapped ions, polar molecules, Rydberg atoms) is that they allow realization of strictly nearest-neighbor hopping¹⁰, thus making it possible to simulate relevant polaron models in a quite realistic fashion. In trapped-ion and polar-molecule systems, for instance, the presence of non-nearest neighbor hopping is unavoidable, originating from the presence of long-range interactions between their elementary constituents (Coulomb interaction between ions and dipolar interaction between polar molecules); these systems show similar limitations when it comes to mimicking the behavior of dispersionless (zero-dimensional) phonons^{5,7,8}. In addition to these intrinsic advantages of superconducting systems compared to other available experimental platforms, a unique aspect of our suggested setup is the capability of the *in-situ* altering of the hopping energy

through an externally-tunable magnetic flux.

Once experimentally realized, our suggested setup could also be used for studying the nonequilibrium aspects of polaron physics, i.e., the dynamics of small-polaron formation. Experimental studies of such phenomena in traditional solid-state systems are hampered by the very short dynamical time scales, in addition to a very limited control over these systems. Our setup paves the way for a controlled experimental investigation of this important phenomenon using a Ramsey-interference protocol. It holds promise to become an invaluable platform for future studies in this direction.

Acknowledgments

Useful discussions with J. Koch, B. Vlastakis, Z. Mineev, L. I. Glazman, and S. M. Girvin are gratefully acknowledged. V.M.S. was supported by the SNSF. M.V. was supported by the Serbian Ministry of Science, project No. 171027. E.D. acknowledges support from Harvard-MIT CUA, the ARO-MURI on Atomtronics, and ARO MURI Quism program. L.T. was supported by NSF-DMR-0956064 and NSF-CCF-0916303. This research was supported in part by NSF PHY11-25915 through a KITP program (V.M.S. and L.T.).

Appendix A: Derivation of the Josephson-coupling term in the rotating frame

In the following, we present derivation of the effective Josephson coupling terms in the rotating frame. We will make use of the fact that $e^{iH_0t/\hbar}a_n e^{-iH_0t/\hbar} = a_n e^{-i\omega_0 t}$, and that, consequently,

$$\begin{aligned} & e^{\frac{i}{\hbar}H_0t} \phi_{n,\text{res}} e^{-\frac{i}{\hbar}H_0t} \\ &= \delta\theta(a_{n+1}e^{-i\omega_0 t} + a_{n+1}^\dagger e^{i\omega_0 t} - a_n e^{-i\omega_0 t} - a_n^\dagger e^{i\omega_0 t}), \end{aligned} \quad (\text{A1})$$

and rely on the smallness of $\delta\theta$ and the RWA. For an arbitrary unitary transformation with a generator S ($S^\dagger = -S$) applied to an analytic operator function $f(A)$ it holds that $e^S f(A) e^{-S} = f(e^S A e^{-S})$. Therefore,

$$\begin{aligned} & e^{\frac{i}{\hbar}H_0t} \cos(\phi_{n,\text{res}}) e^{-\frac{i}{\hbar}H_0t} = \cos\left(\delta\theta(a_{n+1}e^{-i\omega_0 t} \right. \\ & \left. + a_{n+1}^\dagger e^{i\omega_0 t} - a_n e^{-i\omega_0 t} - a_n^\dagger e^{i\omega_0 t})\right), \end{aligned} \quad (\text{A2})$$

with an analogous relation for $\sin(\phi_{n,\text{res}})$.

We start from an expression for the Josephson coupling obtained by inserting Eq. (2) into Eq. (7). By immediately dropping the terms that will be rapidly rotating

upon transformation to the rotating frame, the remaining Josephson coupling reads

$$\begin{aligned} H_n^J \approx & - \left(2E_J \cos \frac{\phi_n^t}{2} + E_{Jb} \cos \phi_{b0} \right) \\ & \times \cos(\varphi_n - \varphi_{n+1}) + \mathcal{O}(\delta\theta^2). \end{aligned} \quad (\text{A3})$$

With the aid of Eq. (3), the term $\cos(\phi_n^t/2)$ can be written as

$$\begin{aligned} \cos \frac{\phi_n^t}{2} = & - \sin \left(\frac{\pi \cos(\omega_0 t)}{2} \right) \frac{\phi_{n,\text{res}}}{2} \\ & + \cos \left(\frac{\pi \cos(\omega_0 t)}{2} \right) + \mathcal{O}(\delta\theta^2), \end{aligned} \quad (\text{A4})$$

where the last two equations have been derived using the asymptotic relations $\cos(\phi_{n,\text{res}}/2) = 1 + \mathcal{O}(\delta\theta^2)$ and $\sin(\phi_{n,\text{res}}/2) = \phi_{n,\text{res}}/2 + \mathcal{O}(\delta\theta^2)$. At the same time, we will utilize the following well-known expansions in terms of Bessel functions of the first kind:⁶⁷

$$\begin{aligned} \cos \left(\frac{\pi \cos(\omega_0 t)}{2} \right) = & \\ & J_0 \left(\frac{\pi}{2} \right) - 2 \sum_{n=1}^{\infty} J_{2n} \left(\frac{\pi}{2} \right) \cos(2n\omega_0 t), \end{aligned} \quad (\text{A5})$$

$$\begin{aligned} \sin \left(\frac{\pi \cos(\omega_0 t)}{2} \right) = & \\ & 2 \sum_{n=1}^{\infty} J_{2n-1} \left(\frac{\pi}{2} \right) (-1)^{n+1} \cos((2n-1)\omega_0 t). \end{aligned} \quad (\text{A6})$$

We now have to analyze which terms in the last two expansions will remain after the transformation to the rotating frame. The first (time-independent) term in Eq. (A5) will clearly be unaffected by this transformation, while the remaining terms rotate at frequency $2\omega_0$ or higher and can therefore be neglected by virtue of the RWA. It is also easy to see that the $n=1$ term in Eq. (A6) will also give rise to time-independent terms. Namely, using Eq. (A1) we straightforwardly obtain

$$\cos(\omega_0 t) e^{\frac{i}{\hbar}H_0t} \phi_{n,\text{res}} e^{-\frac{i}{\hbar}H_0t} = \frac{\phi_{n,\text{res}}}{2} + \dots, \quad (\text{A7})$$

where the ellipses stand for the terms that rotate at frequency $2\omega_0$, and can therefore be neglected. In this manner, after choosing $E_{Jb} = 2E_J J_0(\pi/2)$, we obtain Eq. (11). It should be stressed that, being approximately given by Eq. (13), the term $\cos(\varphi_n - \varphi_{n+1})$ is unaffected by the transformation to the rotating frame.

¹ R. P. Feynman, Int. J. Theor. Phys. **21**, 467 (1982).

² S. Lloyd, Science **273**, 1073 (1996).

- ³ J. I. Cirac and P. Zoller, *Nature Phys.* **8**, 264 (2012).
- ⁴ For a recent review, see I. M. Georgescu, S. Ashhab, and F. Nori, *Rev. Mod. Phys.* **86**, 153 (2014).
- ⁵ V. M. Stojanović, T. Shi, C. Bruder, and J. I. Cirac, *Phys. Rev. Lett.* **109**, 250501 (2012).
- ⁶ A. Mezzacapo, J. Casanova, L. Lamata, and E. Solano, *Phys. Rev. Lett.* **109**, 200501 (2012).
- ⁷ F. Herrera and R. V. Krems, *Phys. Rev. A* **84**, 051401 (2011).
- ⁸ F. Herrera, K. W. Madison, R. V. Krems, and M. Berciu, *Phys. Rev. Lett.* **110**, 223002 (2013).
- ⁹ J. P. Hague and C. MacCormick, *New J. Phys.* **14**, 033019 (2012); *Phys. Rev. Lett.* **109**, 223001 (2012).
- ¹⁰ F. Mei, V. M. Stojanović, I. Siddiqi, and L. Tian, *Phys. Rev. B* **88**, 224502 (2013).
- ¹¹ L. D. Landau, *Z. Phys.* **3**, 664 (1933); S. I. Pekar, *Zh. Eksp. Teor. Fiz.* **16**, 341 (1946).
- ¹² A. S. Alexandrov and J. T. Devreese, *Advances in Polaron Physics* (Springer-Verlag, Berlin, 2010).
- ¹³ S. A. Baily and D. Emin, *Phys. Rev. B* **73**, 165211 (2006).
- ¹⁴ K. Agarwal, I. Martin, M. D. Lukin, and E. Demler, *Phys. Rev. B* **87**, 144201 (2013).
- ¹⁵ C. P. Adams, J. W. Lynn, Y. M. Mukovskii, A. A. Arsenov, and D. A. Shulyatev, *Phys. Rev. Lett.* **85**, 3954 (2000).
- ¹⁶ O. Rösch, O. Gunnarsson, X. J. Zhou, T. Yoshida, T. Sasagawa, A. Fujimori, Z. Hussain, Z.-X. Shen, and S. Uchida, *Phys. Rev. Lett.* **95**, 227002 (2005).
- ¹⁷ See, e.g., L. Mathey, D.-W. Wang, W. Hofstetter, M. D. Lukin, and E. Demler, *Phys. Rev. Lett.* **93**, 120404 (2004); I. E. Mazets, G. Kurizki, N. Katz, and N. Davidson, *ibid.* **94**, 190403 (2005); F. M. Cucchietti and E. Timmermans, *ibid.* **96**, 210401 (2006); A. A. Blinova, M. G. Boshier, and E. Timmermans, *Phys. Rev. A* **88**, 053610 (2013).
- ¹⁸ T. Holstein, *Ann. Phys. (N.Y.)* **8**, 343 (1959).
- ¹⁹ V. M. Stojanović, P. A. Bobbert, and M. A. J. Michels, *Phys. Rev. B* **69**, 144302 (2004).
- ²⁰ S. Ciuchi and S. Fratini, *Phys. Rev. Lett.* **106**, 166403 (2011); N. Vukmirović, C. Bruder, and V. M. Stojanović, *ibid.* **109**, 126407 (2012).
- ²¹ L. M. Woods and G. D. Mahan, *Phys. Rev. B* **61**, 10651 (2000).
- ²² N. Vukmirović, V. M. Stojanović, and M. Vanević, *Phys. Rev. B* **81**, 041408(R) (2010); V. M. Stojanović, N. Vukmirović, and C. Bruder, *ibid.* **82**, 165410 (2010).
- ²³ B. Gerlach and H. Löwen, *Phys. Rev. B* **35**, 4291 (1987); **35**, 4297 (1987).
- ²⁴ C. Slezak, A. Macridin, G. A. Sawatzky, M. Jarrell, and T. A. Maier, *Phys. Rev. B* **73**, 205122 (2006).
- ²⁵ M. H. Devoret and R. J. Schoelkopf, *Science* **339**, 1169 (2013); J. Q. You and F. Nori, *Nature (London)* **474**, 589 (2011); J. Clarke and F. K. Wilhelm, *Nature (London)* **453**, 1031 (2008).
- ²⁶ A. Wallraff *et al.*, *Nature (London)* **431**, 162 (2004).
- ²⁷ A. Blais, R.-S. Huang, A. Wallraff, S. M. Girvin, and R. J. Schoelkopf, *Phys. Rev. A* **69**, 062320 (2004).
- ²⁸ For an introduction, see S. M. Girvin, in *Lecture Notes on Strong Light-Matter Coupling: from Atoms to Solid-State Systems* (World Scientific, Singapore, 2013).
- ²⁹ L. DiCarlo *et al.*, *Nature (London)* **460**, 240 (2009).
- ³⁰ V. M. Stojanović, A. Fedorov, A. Wallraff, and C. Bruder, *Phys. Rev. B* **85**, 054504 (2012).
- ³¹ For an overview, see A. A. Houck, H. E. Türeci, and J. Koch, *Nature Phys.* **8**, 292 (2012).
- ³² S. Schmidt and J. Koch, *Ann. Phys.* **525**, 395 (2013).
- ³³ H. Paik *et al.*, *Phys. Rev. Lett.* **107**, 240501 (2011).
- ³⁴ C. Rigetti *et al.*, *Phys. Rev. B* **86**, 100506(R) (2012).
- ³⁵ M. Hohenadler, M. Aichhorn, L. Pollet, and S. Schmidt, *Phys. Rev. A* **85**, 013810 (2012).
- ³⁶ A. A. Gangat, I. P. McCulloch, and G. J. Milburn, *Phys. Rev. X* **3**, 031009 (2013).
- ³⁷ B. Villalonga Correa, A. Kurcz, and J. J. Garcia-Ripoll, *J. Phys. B: At. Mol. Opt. Phys.* **46**, 224024 (2013).
- ³⁸ L. Tian, *Phys. Rev. Lett.* **105**, 167001 (2010).
- ³⁹ Y. Zhang, L. Yu, J.-Q. Liang, G. Chen, S. Jia, and F. Nori, *Nature Sci. Rep.* **4**, 4083 (2014).
- ⁴⁰ U. Las Heras, A. Mezzacapo, L. Lamata, S. Filipp, A. Wallraff, and E. Solano, arXiv:1311.7626.
- ⁴¹ D. J. Egger and F. K. Wilhelm, *Phys. Rev. Lett.* **111**, 163601 (2013).
- ⁴² A. Kurcz, A. Bermudez, and J. J. Garcia-Ripoll, arXiv:1310.8173.
- ⁴³ T. L. Schmidt, A. Nunnenkamp, and C. Bruder, *New J. Phys.* **15**, 025043 (2013).
- ⁴⁴ E. Kapit, *Phys. Rev. A* **87**, 062336 (2013).
- ⁴⁵ J. Koch *et al.*, *Phys. Rev. A* **76**, 042319 (2007).
- ⁴⁶ D. Emin and M. A. Kriman, *Phys. Rev. B* **34**, 7278 (1986).
- ⁴⁷ L.-C. Ku and S. A. Trugman, *Phys. Rev. B* **75**, 014307 (2007).
- ⁴⁸ G. Li, B. Movaghar, and M. A. Ratner, *Phys. Rev. B* **87**, 094302 (2013).
- ⁴⁹ Z. Feng, V. Timoshevskii, A. Mauger, C. M. Julien, K. H. Bevan, and K. Zaghbi, *Phys. Rev. B* **88**, 184302 (2013).
- ⁵⁰ M. H. Devoret, in *Quantum Fluctuations*, S. Reynaud, E. Giacobino, J. Zinn-Justin, Eds. (Elsevier, Amsterdam, 1997).
- ⁵¹ T. P. Orlando and K. A. Delin, *Introduction to Applied Superconductivity* (Addison-Wesley, Reading, 1991).
- ⁵² See, e.g., Y. Makhlin, G. Schön, and A. Shnirman, *Rev. Mod. Phys.* **73**, 357 (2001).
- ⁵³ S. Johnston, F. Vernay, B. Moritz, Z.-X. Shen, N. Nagaosa, J. Zaanen, and T. P. Devereaux, *Phys. Rev. B* **82**, 064513 (2010).
- ⁵⁴ Z. Radović, N. Božović, and I. Božović, *Phys. Rev. B* **77**, 092508 (2008).
- ⁵⁵ V. Y. Butko, G. Logvenov, N. Božović, Z. Radović, and I. Božović, *Adv. Mat.* **21**, 3644 (2009).
- ⁵⁶ A. Alvermann, D. M. Edwards, and H. Fehske, *Phys. Rev. Lett.* **98**, 056602 (2007).
- ⁵⁷ V. M. Stojanović and M. Vanević, *Phys. Rev. B* **78**, 214301 (2008); see also D. J. J. Marchand *et al.*, *Phys. Rev. Lett.* **105**, 266605 (2010).
- ⁵⁸ J. K. Cullum and R. A. Willoughby, *Lanczos Algorithms for Large Symmetric Eigenvalue Computations* (Birkhäuser, Boston, 1985).
- ⁵⁹ G. Wellein and H. Fehske, *Phys. Rev. B* **56**, 4513 (1997).
- ⁶⁰ M. Marthaler, G. Schön, and A. Shnirman, *Phys. Rev. Lett.* **101**, 147001 (2008).
- ⁶¹ S. Engelsberg and J. R. Schrieffer, *Phys. Rev.* **131**, 993 (1963).
- ⁶² J. M. Gambetta, F. Motzoi, S. T. Merkel, and F. K. Wilhelm, *Phys. Rev. A* **83**, 012308 (2011).
- ⁶³ See, e.g., R. Fazio, G. M. Palma, and J. Siewert, *Phys. Rev. Lett.* **83**, 5385 (1999).
- ⁶⁴ G. De Chiara, T. Calarco, S. Fishman, and G. Morigi, *Phys. Rev. A* **78**, 043414 (2008).
- ⁶⁵ M. Knap, A. Kantian, T. Giamarchi, I. Bloch, M. D. Lukin, and E. Demler, *Phys. Rev. Lett.* **111**, 147205 (2013).
- ⁶⁶ G. S. Paraoanu, *Phys. Rev. Lett.* **97**, 180406 (2006).

⁶⁷ G. B. Arfken and H. J. Weber, *Mathematical Methods for Physicists* (Academic Press, San Diego, 2001), 5th ed.